Letter

Observation of edge-to-edge topological transport in a photonic lattice

Weijie Liu,[1,*] Chaohua Wu,[2,3,*] Yuechen Jia,[1] Suotang Jia,[2,3] Gang Chen,[2,3,4,†] and Feng Chen[1,‡]

[1]*School of Physics, State Key Laboratory of Crystal Materials, Shandong University, Jinan 250100, China*

[2]*State Key Laboratory of Quantum Optics and Quantum Optics Devices, Institute of Laser Spectroscopy, Shanxi University, Taiyuan 030006, China*

[3]*Collaborative Innovation Center of Extreme Optics, Shanxi University, Taiyuan 030006, China*

[4]*Collaborative Innovation Center of Light Manipulations and Applications, Shandong Normal University, Jinan 250358, China*

(Received 9 January 2022; accepted 2 June 2022; published 16 June 2022)

The edge-to-edge topological transport of the one-dimensional odd-sized Su-Schrieffer-Heeger model plays a crucial role in robust energy transfer and information processing. However, it has not been verified experimentally. Here we report on an experimental demonstration of this topological transport in a one-dimensional photonic lattice of coupled waveguides. When slowly varying the spacings of the adjacent waveguides, the robust topological transport of light from the leftmost to the rightmost channels has been successfully observed. Moreover, the transport speed and efficiency of light are enhanced considerably by introducing the exponential-type modulations of the coupling strengths. The experimental results agree well with analytical calculations and numerical simulations. This transport of light observed may serve as the basis for photonic devices of unconventional functions.

DOI: 10.1103/PhysRevA.105.L061502

The discovery of topological insulators opens a new route to explore exotic transport phenomena in a range of physical platforms, including electronic systems [1,2], photonics [3,4], acoustics [5,6], ultracold atoms [7,8], and others [9–12]. One of the hallmark features of the topological insulators is the existence of the nontrivial edge states at the boundaries, providing an intriguing way to route energy and information [13–19]. Such topological transports offer immunity against scattering from disorders and imperfections, and thus have promising applications in designing novel low-loss devices [20–23] and implementing quantum computing [24,25]. So far, the two-dimensional (2D) Chern insulators with 1D chiral edge states are the most reliable designs for realizing the topological transports [26–30].

As the most fundamental topological insulator model, the 1D Su-Schrieffer-Heeger (SSH) lattice can host 0D edge states [31]. Particularly, for the odd-sized case, it only has one edge state but with the tunable localized position [32]. This feature inspires us to achieve topological transport by adiabatically pumping the edge state from one side to the other (called edge-to-edge topological transport) [33,34]. In contrast to the conventional Thouless pumping [35–43], such topological transport is controlled only by the coupling strengths without introducing additional modulations of the on-site energies (Rice-Mele model). Moreover, this protocol has the distinct advantage that both the transport speed and efficiency can be substantially enhanced by designing the suitable modulation functions of the coupling strengths [44]. Such fast and high-efficiency edge-to-edge topological transport plays a crucial role in robust energy transfer and information processing [45–49]. However, this novel topological transport has not been verified experimentally.

In this work, we report on an experimental demonstration of the above edge-to-edge topological transport in a 1D photonic lattice of coupled waveguides. By fabricating an odd-sized SSH model with both the spatially modulated intracell and intercell coupling strengths, the robust topological transport of light from the leftmost to the rightmost channels are successfully observed. Moreover, the transport speed and efficiency of light are enhanced considerably by introducing the exponential-type modulations of the coupling strengths. The experimental results are in good agreement with analytical calculations and numerical simulations. The novel transport of light observed may serve as the basis for photonic devices of unconventional functions.

Figure 1(a) shows a schematic illustration for implementing a 1D SSH model in an array of evanescently coupled waveguides. The waveguide array with a total length L has $2N-1$ (odd-sized) sites, i.e., the system has N complete unit cells minus one end site. Each unit cell contains two sublattice sites A and B. Both the intracell and intercell coupling strengths (J_1 and J_2) are modulated along the propagation distance (z). Under the tight-binding approximation, the propagation of light in this waveguide array is governed by the following Schrödinger-type equation: $-i\partial_z|\psi(z)\rangle = H(z)|\psi(z)\rangle$, with the Hamiltonian

$$H(z) = \sum_n [J_1(z)|n, A\rangle\langle n, B| + J_2(z)|n+1, A\rangle\langle n, B| + \text{H.c.}], \quad (1)$$

*These authors contributed equally to this work
†chengang971@163.com
‡drfchen@sdu.edu.cn

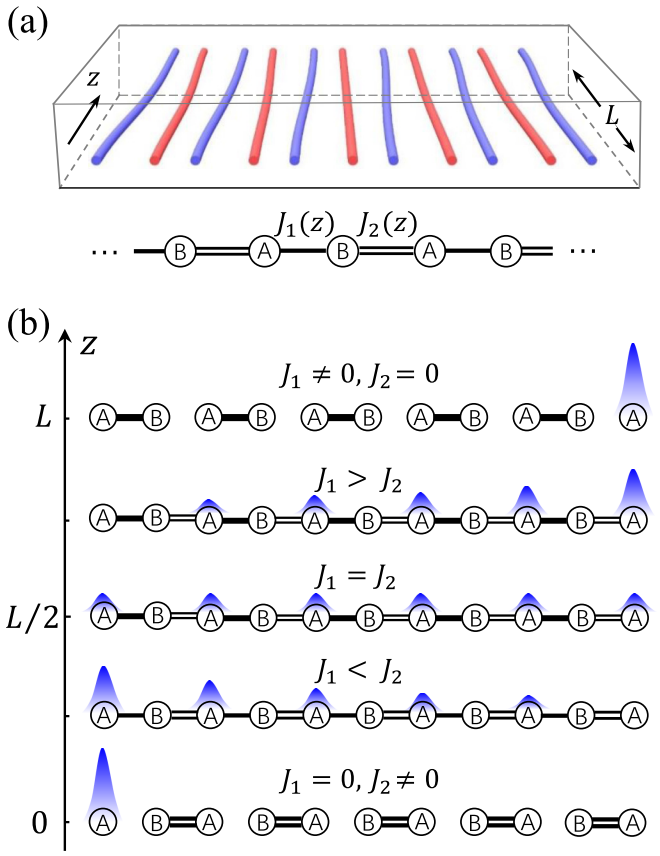

FIG. 1. (a) Schematic illustration of a 1D waveguide array for implementing an odd-sized SSH model with two sublattice sites, A (blue) and B (red), and z-dependent intracell and intercell coupling strengths labeled, respectively, by $J_1(z)$ and $J_2(z)$. The zero-energy edge state of this model only occupies the A-type waveguides [see Eq. (2)]. (b) Schematic illustration of an edge-to-edge topological transport of light by adiabatically modulating the coupling strengths from $J_1(z=0)=0$ and $J_2(z=0)\neq 0$ to $J_1(z=L)\neq 0$ and $J_2(z=L)=0$. The blue-gradient wave packets indicate the distributions of the zero-energy edge states for the different propagation distances.

where $|\psi(z)\rangle$ is a wave function corresponding to the electric-field envelope, n is an index of the unit cell, and H.c. represents the Hermitian conjugate.

The Hamiltonian (1) obeys the chiral symmetry, since $\Gamma H \Gamma^{-1} = -H$, where the chiral operator $\Gamma = \mathbb{I} \otimes \sigma_z$ with $\mathbb{I}$ and σ_z being the $N \times N$ identity and Pauli matrices. This chiral symmetry ensures that a topologically protected zero-energy edge state always exists in the odd-sized waveguide array [32]. When $J_1 < J_2$ or $J_1 > J_2$, the edge state is localized at the left or right side of the waveguide array. The wave functions for the left and right edges are given, respectively by

$$|\psi_l\rangle = \mathcal{N}_l \sum_n (-J_1/J_2)^{n-1} |n, A\rangle, \tag{2a}$$

$$|\psi_r\rangle = \mathcal{N}_r \sum_n (-J_2/J_1)^{N-n} |n, A\rangle, \tag{2b}$$

where $\mathcal{N}_l$ and $\mathcal{N}_r$ are the normalized coefficients. See Supplemental Material I (SM-I) [50] for more details. Equation (2) shows that the edge state only occupies the A-type waveguides. In the limit case of $J_1/J_2 \to 0$ ($J_2/J_1 \to 0$), $|\psi_l\rangle = |1, A\rangle$ ($|\psi_r\rangle = |N, A\rangle$), showing that the edge state is localized at the leftmost (rightmost) waveguide. At $J_1 = J_2$, the zero-energy eigenstate is fully delocalized along the waveguide array.

The nontrival feature of the odd-sized SSH model inspires us to realize an edge-to-edge topological transport of light through modulating J_1 and J_2. As shown in Fig. 1(b) or SM-II [50], the system is initially prepared with $J_1(z=0) = 0$ and $J_2(z=0) = J_m$, where J_m is the maximum value of both the modulated J_1 and J_2. Moreover, the injected light is launched at the leftmost waveguide, which overlaps with the zero-energy edge state $|\psi(z=0)\rangle = |1, A\rangle$. Then, by slowly modulating the coupling strengths from $J_1/J_2 < 1$ to $J_1/J_2 > 1$, the light propagates adiabatically from $|\psi_l\rangle$ to $|\psi_r\rangle$ along the zero-energy eigenstates. Finally, the coupling strengths have $J_1(z=L) = J_m$ and $J_2(z=L) = 0$, at which the light arrives at the rightmost waveguide with the zero-energy edge state $|\psi(z=L)\rangle = |N, A\rangle$. Noticeably, this topologically protected transfer of light requires adiabatic evolution of the Hamiltonian (1). To approach the adiabatic limit, we have

$$\sum_{l\neq 0} \frac{\langle \psi_0(z)|\partial H(z)/\partial z|\psi_l(z)\rangle}{E_l(z) - E_0(z)} \ll 1, \tag{3}$$

where $|\psi_l(z)\rangle$ is the instantaneous eigenstate of the lth mode with eigenenergy $E_l(z)$. It follows from Eq. (3) that the temporal variations of J_1 and J_2 should be much slower than the energy gap (Δ) between the zero-energy and its adjacent eigenstates. It should be noticed that, for infinite system size, the energy gap vanishes at $z = L/2$ ($J_1 = J_2$). However, a finite minimum energy gap is always present for finite system, which is important for the realization of efficient topological transport.

We emphasize that this edge-to-edge topological transport is controlled only by J_1 and J_2, in contrast to the even case that the topological transport of the Thouless pumping is generated by introducing additional modulations of the on-site energies [37–40]. Moreover, during the evolution of the system, the energy gap of the Thouless pumping is quite small over a wide range even for finite-sized lattice [35,51]. These require that the temporal variation of the system Hamiltonian is extremely slow. Our protocol provides a convenient way to speed up the transport process by engineering appropriate modulation functions. Specifically, the introduction of the exponential modulations of J_1 and J_2 not only increases the minimum value of the energy gap, but also suitably adapts the slope of the modulated functions based on the value of the instantaneous energy gap [i.e., J_1 and J_2 have a smaller (steeper) slope for small (large) energy gap] [44]. As a result, the transport speed and efficiency of light can be enhanced considerably. See SM-III [50] for more details.

Having illustrated the fundamental protocol how to realize the edge-to-edge topological transport of light, we perform relevant experiments in photonic waveguide arrays, which are fabricated in borosilicate glass (Eagle XG) using direct femtosecond-laser-writing technology. The borosilicate glass is mounted on a 3D x-y-z translation stage. The femtosecond laser (Femto YL-25, YSL Photonics) has a wavelength of

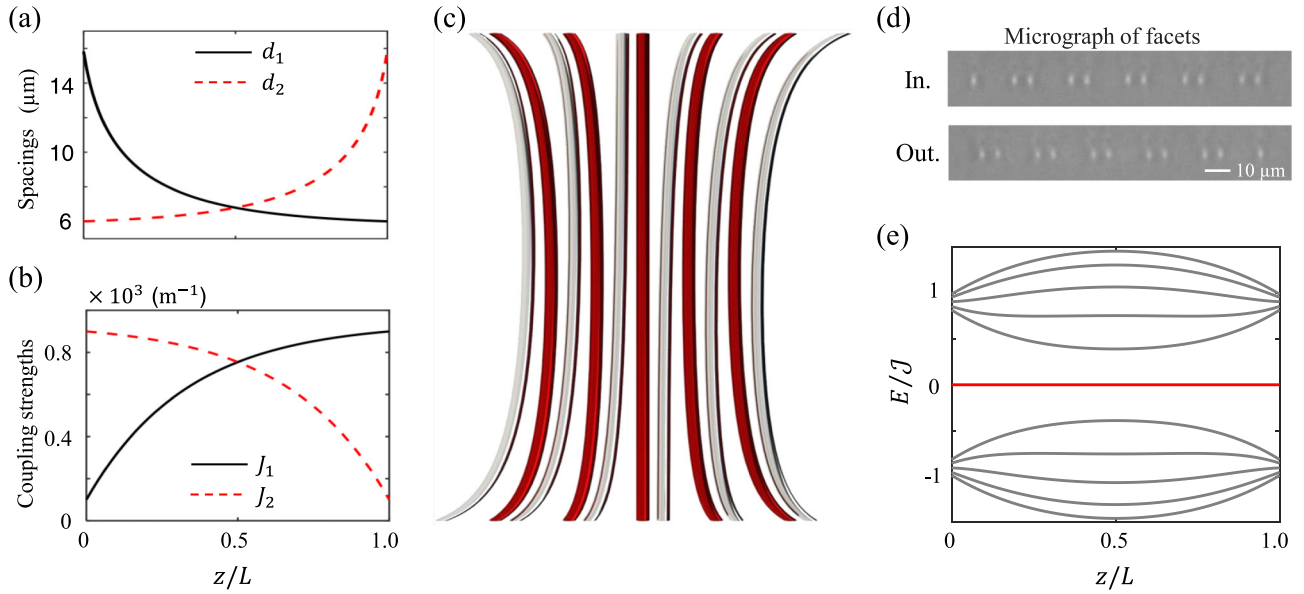

FIG. 2. (a) Intracell (black solid curve) and intercell (red dashed curve) spacings, d_1 and d_2, as functions of z. (b) The coupling strength J_1 and J_2 as functions of z. (c) Schematic of the exponential-type modulated waveguide array structure. (d) Micrograph of the input (upper panel) and output (lower panel) facets of the fabricated waveguide array. (e) Energy spectra of the coupled waveguides. The red solid line in the gap denotes the zero-energy edge states.

1030 nm, a pulse duration of 400 fs, and a repetition rate of 2.5 MHz. A microscope objective (50/0.45) is utilized to focus the beam to 230 μm below the substrate surface of the sample. The pulse energy is adjusted to 212 nJ and the writing speed is set to 1 mms^{-1}. The width of the fabricated waveguide is $\sim$4 μm, and the refractive index difference Δn is $\sim 10^{-3}$. The coupling strengths are determined by the spacings of the adjacent waveguides. In addition, the laser with a wavelength of 633 nm is injected into the leftmost waveguide and the output intensity distribution is measured at the output facet using a CCD camera.

To realize the exponential modulations of J_1 and J_2, we vary d_1 and d_2 by continuously moving the sample through a high-precision system. In the fabricated waveguide array with the 633 nm injected laser, it exists a general relation between the coupling strength and the spacing: $J = \eta e^{\gamma d}$, where $\eta = 3451$ m^{-1} and $\gamma = -0.2238$ μm^{-1} [50]. As a result, for the z-dependent d_1 (black solid curve) and d_2 (red dashed curve) in Fig. 2(a), the exponential modulations [Fig. 2(b)] are achieved as

$$J_1 = \mathcal{J}[0.1 + 0.8(1 - e^{-3z/L})/(1 - e^{-3})],$$
$$J_2 = \mathcal{J}\{0.1 + 0.8[(1 - e^{-3(L-z)/L})]/(1 - e^{-3})\},$$

where the coefficient $\mathcal{J} = 1000$ m^{-1}. Note that in order to avoid loss caused by the large bending of the waveguides, the minimum and maximum spacings are set to 6 and 16 μm, respectively, i.e., both J_1 and J_2 have added a factor of 0.1, compared with the theoretical proposal in SM-III [50]. A sketch of such a waveguide array is shown in Fig. 2(c). The width of the waveguide array varies with the propagation distance, and approaches its minimum value at $z = L/2$. Figure 2(d) shows the micrograph of the input ($z = 0$) and output ($z = L$) facets of the fabricated waveguide array with 11 sites ($N = 6$). This figure exhibits a realization of the odd-sized SSH Hamiltonian (1). As shown in Fig. 2(e), we plot energy spectrum of the fabricated waveguide array with the exponential modulations. Clearly, such waveguide array exhibits a zero-energy edge state and the energy gap approaches its minimum value at $z = L/2$.

In Figs. 3(a) and 3(b), we further calculate $|\psi(z)|^2$ of the corresponding waveguide array with 11 sites ($N = 6$) by both the coupled-mode theory [52,53] and the Beam Propagation Method through software Rsoft®. It can be seen that when the light is injected to the first (leftmost) site with the wave function $|1, A\rangle$, it is pumped adiabatically along the zero-energy edge states only occupying the A-type waveguides when slowly modulating J_1 and J_2. Finally, the light arrives at the output localized at the eleventh (rightmost) site with the wave function $|6, A\rangle$. This is consistent with the previous tight-binding analysis in Fig. 1(b). In the experiment, to record the intensity distributions inside the structure at the specific distance (see, for example, $L/4$), we directly fabricate a waveguide array with the length $L/4$, and then observe the corresponding light intensity of the output. In Fig. 3(c), we measure the intensity distributions of light at different stages of the adiabatic evolution (i.e., different propagation distances $z = 0, L/4, L/2, 3L/4, L$ with $L = 5$ cm). This experimental observation, agreeing well with the numerical simulations in Figs. 3(a) and 3(b), demonstrates clearly the expected edge-to-edge topological transport of light.

In Fig. 4(a), we fabricate various waveguide array samples with different total propagation length L, and present the measured outgoing intensity distributions of light for $L \in [1, 5]$ cm with an interval of 0.5 cm, when the injected light is launched at the leftmost waveguide. It can be seen that when $L = 1$ cm, the injected light is distributed throughout the array at the output. This is due to the nonadiabatic evolution for small L, i.e., the population of the zero-energy edge state transits quickly to other eigenstates and fails to return;

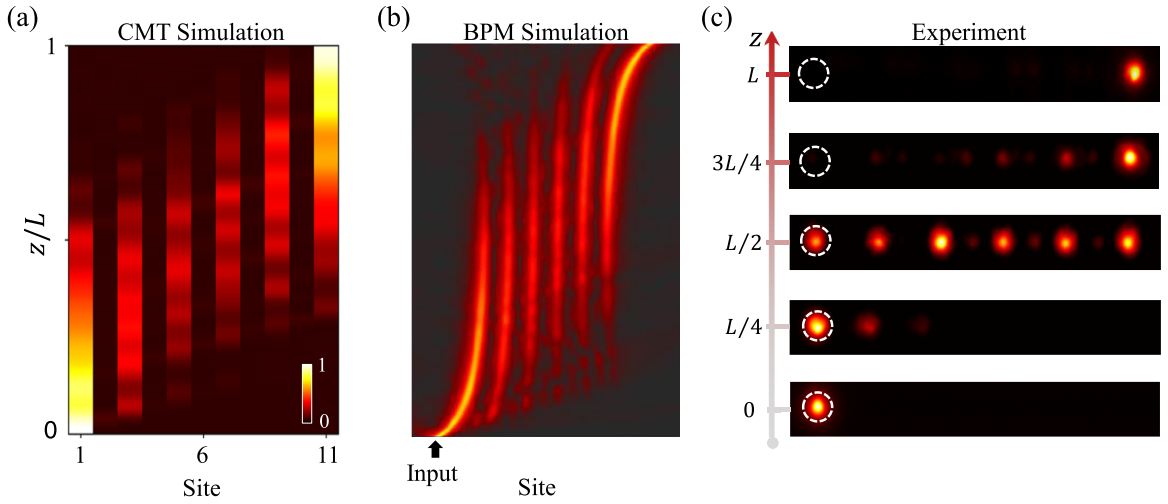

FIG. 3. (a), (b) Calculations of $|\psi(z)|^2$ for $L = 5$ cm, based on the coupled-mode theory (CMT) and the beam propagation method (BPM). (c) Measured intensity distributions of light for $z = 0$, $L/4$, $L/2$, $3L/4$, L with the same length as in (a) and (b). The white dashed circles indicate the injection sites at the input facet ($z = 0$). To better illustrate the transport of light in the curved waveguide array, the scale ratio between the horizontal and vertical direction in (b) is about 1/230. The site is chosen as 11.

see SM-III for details [50]. When $L > 1$ cm, the evolution approaches to the adiabatic condition and the output light is concentrated mostly in the rightmost waveguide, indicating the emergence of the edge-to-edge topological transport of light. As a comparison, we implement another protocol of the cosine modulations, i.e., $J_1 = \mathcal{J}\{0.1 + 0.4[1 - \cos(\pi z/L)]\}$ and $J_2 = \mathcal{J}\{0.1 + 0.4[1 + \cos(\pi z/L)]\}$. Note that the minimum and maximum spacings are also set to 6 and 16 μm, respectively. In Fig. 4(b), we measure the corresponding outgoing intensity distributions of light, showing that the emergence of the edge-to-edge topological transport of light (i.e., the intensity of the rightmost waveguide dominates) requires $L > 3$ cm. Compared Fig. 4(a) with Fig. 4(b), it can be found that the realization of the edge-to-edge topological transport of light by the exponential modulations requires a shorter length than that by the cosine modulations, i.e., the transport speed of light for the exponential modulations is faster than that for the cosine modulations.

We further introduce a relative quantity

$$\mathcal{F} = |\langle N, A|\psi(z = L)\rangle|^2/|\psi(z = L)|^2 = I_{\text{out}}^{\text{R}}/I_{\text{out}}^{\text{T}}, \quad (4)$$

i.e., the ratio of the intensity of the rightmost waveguide at the output facet to that of the total outgoing intensity. This relative quantity can effectively reflect the localization of light at the rightmost waveguide, and thus characterize its transport efficiency [54]. In Fig. 4(c), we measure $\mathcal{F}$ as functions of L for both the exponential (red circles) and cosine (black squares) modulations, which are in agreement with the theoretical calculations (solid lines) from the tight-binding Hamiltonian (1). This figure exhibits the faster property of the exponential modulations again. Moreover, for a shorter $L = 1.5$ cm, the transport efficiency for the exponential modulations is

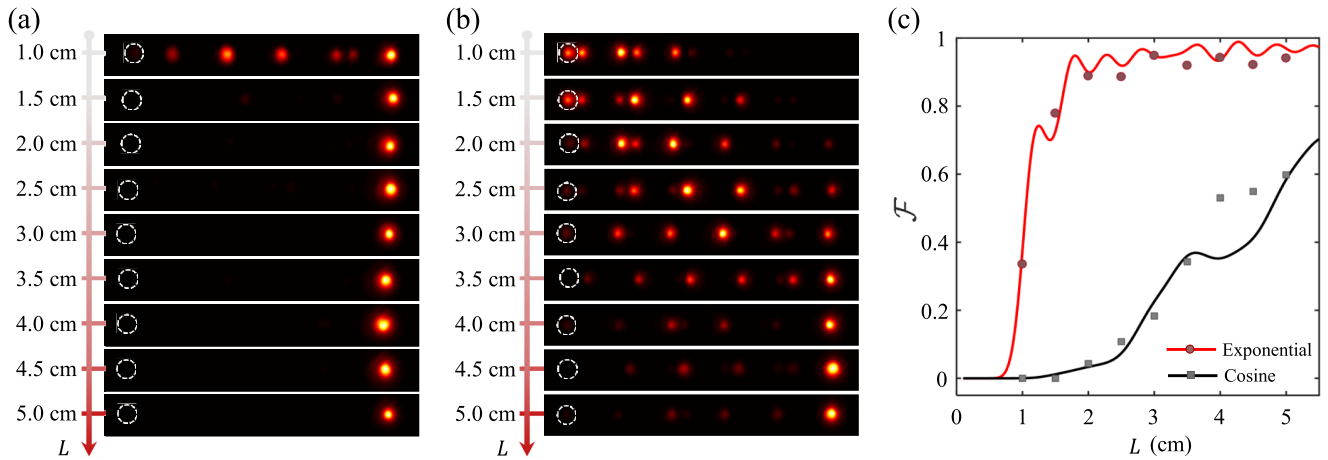

FIG. 4. (a), (b) Measured profiles of the output intensity distributions of light for the exponential (a) and cosine (b) modulations, when $L \in [1, 5]$ cm with an interval of 0.5 cm. The white dashed circles denote the injection sites at the input facet ($z = 0$). (c) Measured transport efficiencies $\mathcal{F}$ as functions of L for the exponential (red circles) and cosine (black squares) modulations. The solid lines show the theoretical calculations from the tight-binding Hamiltonian (1). The site is the same as that in Fig. 3.

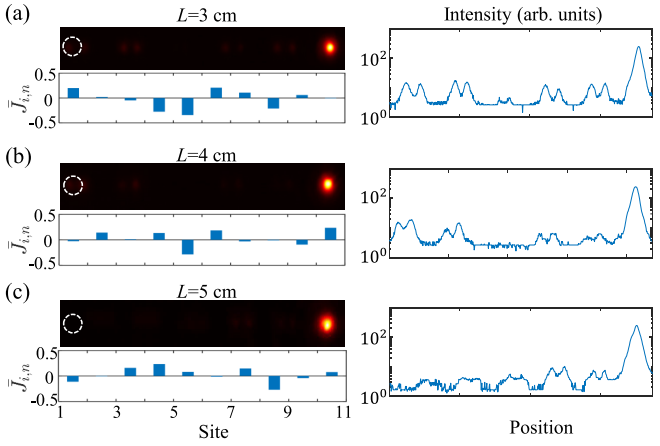

FIG. 5. Measured profiles of the output intensity distributions of light (upper panels) for the weak disorders when $L = 3$ (a), 4 (b), 5 cm (c). The white dashed circles indicate the injection sites at the input facet ($z = 0$). The lower panels in all subfigures show the corresponding disorder distributions of the coupling strengths, generated randomly with $W = 0.8$. The right panels show the output intensity profile of the light in the waveguide array. The site is the same as that in Fig. 3.

$\mathcal{F} \sim 0.78$, which can be enhanced by increasing L. For example, when $L = 4$ cm, $\mathcal{F} \sim 0.94$. Notably, the transport efficiency of the exponential modulations is always higher than that of the cosine modulations.

Finally, we experimentally demonstrate the robustness of the edge-to-edge topological transport of light by introducing random fluctuations to the exponential-type coupling strengths (i.e., off-diagonal disorder). In this case, the total Hamiltonian

$$\mathcal{H} = \sum_n [J_1(z)(1+\bar{J}_{1,n})|n,A\rangle\langle n,B| + J_2(z)(1+\bar{J}_{2,n})|n+1,A\rangle\langle n,B| + \text{H.c.}], \quad (5)$$

where $\bar{J}_{i,n} = W\delta$ $(i = 1, 2)$ with W being a disorder strength and $\delta \in [-0.5, 0.5]$ being a uniformly distributed random number. The perturbed Hamiltonian $\mathcal{H}$ still obeys the chiral symmetry, i.e., $\Gamma\mathcal{H}\Gamma^{-1} = -\mathcal{H}$, implying that the zero-energy edge state is not affected by such disorder. In Fig. 5, we measure the outgoing intensity distributions of light when the disorders are imposed, respectively, on each coupling terms of the waveguide array. This figure shows that for the weak disorder, the injected light can propagate well from the leftmost to the rightmost channels along the zero-energy edge states, demonstrating definitely the robustness of the edge-to-edge topological transport of light. This is a universal property induced by the intrinsic feature of the topological insulator. For strong disorder, the transport efficiency reduces significantly due to the decreasing of the energy gap. If we consider the diagonal disorder (on-site energies), the perturbed Hamiltonian (5) becomes $\mathcal{H} = H(z) + \sum_n \mathcal{J}(\bar{J}_{1,n}|n,A\rangle\langle n,A| + \bar{J}_{2,n}|n,B\rangle\langle n,B|)$. In this case, the perturbed Hamiltonian does not obey the chiral symmetry and the energy of the edge mode in the gap is modified. However, the main influence of this diagonal disorder on the edge-to-edge topological transport is similar to that of the off-diagonal disorder [50].

In summary, we have reported an experimental observation of an edge-to-edge topological transport of light in a 1D photonic lattice of coupled waveguides, based on the odd-sized SSH model. Such topological transport depends crucially on the spatially modulated coupling strengths (i.e., the interwaveguide spacings). Especially, for the exponential modulations, the transport speed and efficiency can be enhanced considerably. We have also demonstrated the robustness of the topological transport against the disorder. Our results not only may serve as the basis for photonic devices of unconventional functions, but also can be extended to other physical systems, such as superconducting circuits, acoustic system, and mechanical vibrations, for novel applications in wave manipulations, quantum state transfer, and quantum information processing.

This work is supported partly by the National Key R&D Program of China (Grant No. 2021YFA1400900), the National Natural Science Foundation of China (Grants No. 12034012, No. 12074232, and No. 12125406), the Natural Science Foundation of Shandong Province (Grant No. ZR2021ZD02), Taishan Scholar Program (Grant No. tspd20210303), and Shanxi "1331 Project".

[1] M. Z. Hasan and C. L. Kane, Colloquium: Topological insulators, Rev. Mod. Phys. **82**, 3045 (2010).
[2] X. L. Qi and S. C. Zhang, Topological insulators and superconductors, Rev. Mod. Phys. **83**, 1057 (2011).
[3] T. Ozawa, H. M. Price, A. Amo, N. Goldman, M. Hafezi, L. Lu, M. C. Rechtsman, D. Schuster, J. Simon, O. Zilberberg, and I. Carusotto, Topological photonics, Rev. Mod. Phys. **91**, 015006 (2019).
[4] M. Kremer, L. J. Maczewsky, M. Heinrich, and A. Szameit, Topological effects in integrated photonic waveguide structures, Opt. Mater. Express **11**, 1014 (2021).
[5] G. Ma, M. Xiao, and C. T. Chan, Topological phases in acoustic and mechanical systems, Nat. Rev. Phys. **1**, 281 (2019).
[6] H. Nassar, B. Yousefzadeh, R. Fleury, M. Ruzzene, A. Alù, C. Daraio, A. N. Norris, G. Huang, and M. R. Haberman, Nonreciprocity in acoustic and elastic materials, Nat. Rev. Mater. **5**, 667 (2020).
[7] N. R. Cooper, J. Dalibard, and I. B. Spielman, Topological bands for ultracold atoms, Rev. Mod. Phys. **91**, 015005 (2019).
[8] D.-W. Zhang, Y.-Q. Zhu, Y. X. Zhao, H. Yan, and S.-L. Zhu, Topological quantum matter with cold atoms, Adv. Phys. **67**, 253 (2018).
[9] J. Ningyuan, C. Owens, A. Sommer, D. Schuster, and J. Simon, Time- and Site-Resolved Dynamics in a Topological Circuit, Phys. Rev. X **5**, 021031 (2015).

[10] T. Karzig, C.-E. Bardyn, N. H. Lindner, and G. Refael, Topological Polaritons, Phys. Rev. X **5**, 031001 (2015).

[11] S. Klembt, T. H. Harder, O. A. Egorov, K. Winkler, R. Ge, M. A. Bandres, M. Emmerling, L. Worschech, T. C. H. Liew, M. Segev, C. Schneider, and S. Höling, Exciton-polariton topological insulator, Nature (London) **562**, 552 (2018).

[12] Roman Süsstrunk and S. D. Huber, Observation of phononic helical edge states in a mechanical topological insulator, Science **349**, 47 (2015).

[13] Z. Wang, Y. Chong, J. D. Joannopoulos, and M. Soljačić, Observation of unidirectional backscattering-immune topological electromagnetic states, Nature (London) **461**, 772 (2009).

[14] Y. Plotnik, M. C. Rechtsman, D. Song, M. Heinrich, J. M. Zeuner, S. Nolte, Y. Lumer, N. Malkova, J. Xu, A. Szameit, Z. Chen, and M. Segev, Observation of unconventional edge states in photonic graphene, Nat. Mater. **13**, 57 (2014).

[15] J. Lu, C. Qiu, L. Ye, X. Fan, M. Ke, F. Zhang, and Z. Liu, Observation of topological valley transport of sound in sonic crystals, Nat. Phys. **13**, 369 (2017).

[16] E. Lustig, S. Weimann, Y. Plotnik, Y. Lumer, M. A. Bandres, A. Szameit, and M. Segev, Photonic topological insulator in synthetic dimensions, Nature (London) **567**, 356 (2019).

[17] Q. Cheng, Y. Pan, H. Wang, C. Zhang, D. Yu, A. Gover, H. Zhang, T. Li, L. Zhou, and S. Zhu, Observation of Anomalous π Modes in Photonic Floquet Engineering, Phys. Rev. Lett. **122**, 173901 (2019).

[18] Q. Wei, X. Zhang, W. Deng, J. Lu, X. Huang, M. Yan, G. Chen, Z. Liu, and S. Jia, 3D Hinge Transport in Acoustic Higher-Order Topological Insulators, Phys. Rev. Lett. **127**, 255501 (2021).

[19] L. J. Maczewsky, B. Höckendorf, M. Kremer, T. Biesenthal, M. Heinrich, A. Alvermann, H. Fehske, and A. Szameit, Fermionic time-reversal symmetry in a photonic topological insulator, Nat. Mater. **19**, 855 (2020).

[20] B. Bahari, A. Ndao, F. Vallini, A. El Amili, Y. Fainman, and B. Kanté, Nonreciprocal lasing in topological cavities of arbitrary geometries, Science **358**, 636 (2017).

[21] G. Harari, M. A. Bandres, Y. Lumer, M. C. Rechtsman, Y. D. Chong, M. Khajavikhan, D. N. Christodoulides, and M. Segev, Topological insulator laser: Theory, Science **359**, eaar4003 (2018).

[22] M. A. Bandres, S. Wittek, G. Harari, M. Parto, J. Ren, M. Segev, D. N. Christodoulides, and M. Khajavikhan, Topological insulator laser: Experiments, Science **359**, eaar4005 (2018).

[23] H. He, C. Qiu, L. Ye, X. Cai, X. Fan, M. Ke, F. Zhang, and Z. Liu, Topological negative refraction of surface acoustic waves in a Weyl phononic crystal, Nature (London) **560**, 61 (2018).

[24] C. Nayak, S. H. Simon, A. Stern, M. Freedman, and S. D. Sarma, Non-Abelian anyons and topological quantum computation, Rev. Mod. Phys. **80**, 1083 (2008).

[25] S. D. Sarma, M. Freedman, and C. Nayak, Topological quantum computation, Phys. Today **59**, 32 (2006).

[26] F. D. M. Haldane, Model for a Quantum Hall Effect without Landau Levels: Condensed-Matter Realization of the "Parity Anomaly", Phys. Rev. Lett. **61**, 2015 (1988).

[27] F. D. M. Haldane and S. Raghu, Possible Realization of Directional Optical Waveguides in Photonic Crystals with Broken Time-Reversal Symmetry, Phys. Rev. Lett. **100**, 013904 (2008).

[28] L. J. Maczewsky, J. M. Zeuner, S. Nolte, and A. Szameit, Observation of photonic anomalous Floquet topological insulators, Nat. Commun. **8**, 13756 (2017).

[29] S. Mukherjee, A. Spracklen, M. Valiente, E. Andersson, P. Ö berg, N. Goldman, and R. R. Thomson, Experimental observation of anomalous topological edge modes in a slowly driven photonic lattice, Nat. Commun. **8**, 13918 (2017).

[30] M. C. Rechtsman, J. M. Zeuner, Y. Plotnik, Y. Lumer, D. Podolsky, F. Dreisow, S. Nolte, M. Segev, and A. Szameit, Photonic Floquet topological insulators, Nature (London) **496**, 196 (2013).

[31] W. P. Su, J. R. Schrieffer, and A. J. Heeger, Solitons in Polyacetylene, Phys. Rev. Lett. **42**, 1698 (1979).

[32] J. K. Asbóh, L. Oroszláy, and A. Páyi, A Short Course on Topological Insulators: Band Structure and Edge States in One and Two Dimensions, *Lecture Notes in Physics* (Springer, Berlin, 2016), Vol. 979.

[33] F. Mei, G. Chen, L. Tian, S.-L. Zhu, and S. Jia, Robust quantum state transfer via topological edge states in superconducting qubit chains, Phys. Rev. A **98**, 012331 (2018).

[34] S. Longhi, Topological pumping of edge states via adiabatic passage, Phys. Rev. B **99**, 155150 (2019).

[35] Y. E. Kraus, Y. Lahini, Z. Ringel, M. Verbin, and O. Zilberberg, Topological States and Adiabatic Pumping in Quasicrystals, Phys. Rev. Lett. **109**, 106402 (2012).

[36] M. Verbin, O. Zilberberg, Y. Lahini, Y. E. Kraus, and Y. Silberberg, Topological pumping over a photonic Fibonacci quasicrystal, Phys. Rev. B **91**, 064201 (2015).

[37] Y. Ke, X. Qin, F. Mei, H. Zhong, Y. S. Kivshar, and C. Lee, Topological phase transitions and Thouless pumping of light in photonic waveguide arrays, Laser Photonics Rev. **10**, 995 (2016).

[38] S. Nakajima, T. Tomita, S. Taie, T. Ichinose, H. Ozawa, L. Wang, M. Troyer, and Y. Takahashi, Topological Thouless pumping of ultracold fermions, Nat. Phys. **12**, 296 (2016).

[39] M. Lohse, C. Schweizer, O. Zilberberg, M. Aidelsburger, and I. Bloch, A Thouless quantum pump with ultracold bosonic atoms in an optical superlattice, Nat. Phys. **12**, 350 (2016).

[40] A. Cerjan, M. Wang, S. Huang, K. P. Chen, and M. C. Rechtsman, Thouless pumping in disordered photonic systems, Light Sci. Appl. **9**, 178 (2020).

[41] O. Zilberberg, S. Huang, J. Guglielmon, M. Wang, K. P. Chen, Y. E. Kraus, and M. C. Rechtsman, Photonic topological boundary pumping as a probe of 4D quantum Hall physics, Nature (London) **553**, 59 (2018).

[42] Y. Ke, S. Hu, B. Zhu, J. Gong, Y. Kivshar, and C. Lee, Topological pumping assisted by Bloch oscillations, Phys. Rev. Research **2**, 033143 (2020).

[43] Marius Jürgensen, S. Mukherjee, and M. Rechtsman, Quantized nonlinear Thouless pumping, Nature (London) **596**, 63 (2021).

[44] N. E. Palaiodimopoulos, I. Brouzos, F. K. Diakonos, and G. Theocharis, Fast and robust quantum state transfer via a topological chain, Phys. Rev. A **103**, 052409 (2021).

[45] R. J. Chapman, M. Santandrea, Z. Huang, G. Corrielli, A. Crespi, M.-H. Yung, R. Osellame, and A. Peruzzo, Experimental perfect state transfer of an entangled photonic qubit, Nat. Commun. **7**, 11339 (2016).

[46] X. Li, Y. Ma, J. Han, T. Chen, Y. Xu, W. Cai, H. Wang, Y. P. Song, Z.-Y. Xue, Z.-q. Yin, and L. Sun, Perfect Quantum State Transfer in a Superconducting Qubit Chain with

Parametrically Tunable Couplings, Phys. Rev. Applied **10**, 054009 (2018).

[47] A. Blanco-Redondo, B. Bell, D. Oren, B. J. Eggleton, and M. Segev, Topological protection of biphoton states, Science **362**, 568 (2018).

[48] Y. Wang, Y.-H. Lu, J. Gao, K. Sun, Z.-Q. Jiao, H. Tang, and X.-M. Jin, Quantum topological boundary states in quasicrystals, Adv. Mater. **31**, 1905624 (2019).

[49] Y. Wang, X.-L. Pang, Y.-H. Lu, J. Gao, Y.-J. Chang, L.-F. Qiao, Z.-Q. Jiao, H. Tang, and X.-M. Jin, Topological protection of two-photon quantum correlation on a photonic chip, Optica **6**, 955 (2019).

[50] See Supplemental Material at http://link.aps.org/supplemental/10.1103/PhysRevA.105.L061502 for the topologically-protected edge state for the old-sized SSH model (SM-I), the adiabatic pumping of edge state in the odd-sized SSH model (SM-II), the choice of the modulating coupling strengths (SM-III), the implementation of the modulated coupling strengths (SM-IV), the energy spectra of the fabricated photonic waveguides (SM-V), the disorder analysis (SM-VI), and the comparison with conventional topological pumping schemes (SM-VII).

[51] L. Qi, G.-L. Wang, S. Liu, S. Zhang, and H.-F. Wang, Engineering the topological state transfer and topological beam splitter in an even-sized Su-Schrieffer-Heeger chain, Phys. Rev. A **102**, 022404 (2020).

[52] F. Lederer, G. I. Stegeman, D. N. Christodoulides, G. Assanto, M. Segev, and Y. Silberberg, Discrete solitons in optics, Phys. Rep. **463**, 1 (2008).

[53] A. Szameit and S. Nolte, Discrete optics in femtosecond-laser-written photonic structures, J. Phys. B **43**, 163001 (2010).

[54] I. L. Garanovich, S. Longhi, A. A. Sukhorukov, and Y. S. Kivshar, Light propagation and localization in modulated photonic lattices and waveguides, Phys. Rep. **518**, 1 (2012).